Platelets modulate inflammation and matrix remodeling in abdominal aortic aneurysm

Wagenhäuser MU*[1], Mulorz J*[1], Krott KJ*[1], Feige T[1], Ehrenberg A[1], Rhee YH[1], Chatterjee M[2], Petzold N[1], Böddeker C[1], Ibing W[1], Krüger I[1], Spin JM[3,4], Tsao PS[3,4], Roseman A[3], Schelzig H[#1], Elvers M[#§1]

* contributed equally
# contributed equally
§ corresponding author

[1] Department of Vascular- and Endovascular Surgery, University Hospital Düsseldorf, Heinrich-Heine University, Düsseldorf, Germany

[2] Department of Pharmacology, Experimental Therapy and Toxicology, University Hospital Tübingen, Tübingen, Germany

[3] VA Palo Alto Health Care System, Palo Alto, CA, United States

[4] Stanford University, Department of Cardiovascular Medicine, Stanford, CA, United States

Short title: Platelet mediated inflammation and ECM remodeling in AAA

Word Count: 6.277

Abstract Word Count: 186

Keywords: platelets; abdominal aortic aneurysm, inflammation, ECM remodeling

Abstract

Abdominal aortic aneurysm (AAA) is a highly lethal disease with progressive dilatation of the abdominal aorta accompanied by degradation and remodelling of the vessel wall due to chronic inflammation. Platelets are small anuclear cells that can release various inflammatory cytokines and biological response modulators when activated. In cardiovascular diseases, platelets are crucial for the inflammatory response but their role in AAA is poorly understood. However, both -experimental and clinical data- strongly suggest that platelet activation may be relevant for AAA formation and progression. Here, we find that platelets play a crucial role in promoting AAA through modulation of inflammation and degradation of the ECM. They are responsible for the up-regulation of *SPP1* (*osteopontin, OPN)* gene expression in macrophages and aortic tissue, which triggers inflammation and remodeling. Further, enhanced platelet activation and pro-coagulant activity results in elevated gene expression of various cytokines, *Mmp9* and *Col1a1* in macrophages. Platelet depletion in experimental murine AAA reduced inflammation and ECM remodeling, with reduced elastin fragmentation and aortic diameter expansion. In conclusion, our data strongly supports the potential relevance of anti-platelet therapy to reduce AAA progression and rupture in AAA patients.

Introduction

Abdominal aortic aneurysm (AAA) is a localized, progressive dilatation of the abdominal aorta caused by chronic inflammation resulting in adverse remodeling of the aortic wall. Well-established risk factors include age, hypertension, male gender, and smoking tobacco cigarettes. In Western countries, the incidence of AAA is ~0.4–0.67% annually and reaches up to 5–10% in men over age 65 (1). As AAA diameter increases, the risk of fatal rupture rises exponentially. Despite remarkable advances in understanding the underlying pathologic mechanisms during the past years, endovascular and open repair remain the only AAA treatment options. Although potential candidates exist, such as metformin, non-invasive drug-based therapies are pending clinical implementation, since prospective randomized trials have either not demonstrated efficacy or are yet to be performed (2-6).

Characteristic features of AAA pathophysiology are the recruitment of infiltrating inflammatory leukocytes, together with the activation of proteolytic enzymes leading to extracellular matrix degradation, which weakens the aortic vessel wall (7, 8). In this context the formation of an intraluminal thrombus (ILT) may be critical for the progress of the disease, since the ILT modulates both, biomechanical parameters and inflammatory processes in the AAA vessel wall (9, 10). The vast majority of AAAs are accompanied by an ILT, although its disease-specific role is still debated (11, 12). The key elements of inflammatory processes and the formation of an ILT suggest that platelets and their activation might play a significant role for AAA initiation and progression, particularly as evidence has accumulated for platelet-based acceleration of various cardiovascular diseases (13).

Various preclinical animal models exist, allowing mechanistic insights into various aspects of AAA disease (14). Of these, the angiotensin-II (Ang-II) infusion model provides features of dissection and aneurysm formation, and has demonstrated a beneficial effect in AAA rupture rates and reduced macrophage recruitment into the AAA wall in response to antiplatelet drugs (15). Further, the platelet integrin $\alpha_{IIb}\beta_3$ inhibitor abciximab and/or a $P2Y_{12}$ receptor antagonist both blocked AAA growth in a rat xenograft aneurysm model (16, 17). To date, no study has explored the role of platelets in the pancreatic porcine elastase (PPE) infusion model. The PPE model reproduces many features of human AAA and was therefore used in this study (14).

Small clinical trials have supported the hypothesis that platelet activation contributes to AAA development and progression, because anti-platelet medication with low-dose aspirin has been shown to be beneficial for patients with small AAAs, as indicated by decreased aneurysm size and less frequent need for surgical repair (18). In patients with large AAAs, platelet activation is enhanced with increased levels of soluble CD40L, TAT complex formation, P-selectin exposure, and fibrinogen binding (19).

In conclusion, both experimental and clinical data strongly suggest that, in AAA, impaired endothelial function causes platelet activation, leading to ILT formation and promoting a

persistent renewal of cellular activity at the luminal interface via aggregation, entrapment, and recruitment of activated platelets, establishing a chronic inflammatory response. Thus, platelet activation may play a pivotal role in AAA formation and progression.

Despite these theoretical considerations and encouraging results in preclinical animal models and small clinical trials, there is a significant lack of understanding on how platelets contribute to AAA development and progression. More insights into the specific role of platelets in AAA disease and their activation mechanisms are urgently needed to allow the development of appropriate anti-platelet targets. Here, we present findings regarding platelet contribution to AAA disease opening the way for potential novel therapies.

Results

Platelet depletion alleviates experimental AAA progression. We induced experimental murine AAA utilizing the porcine pancreatic elastase (PPE) model and performed platelet depletion by administrating an anti-platelet antibody (or control polyclonal immunoglobulins) at days 0 and 5 following surgery (Figure 1 A and B). We found that platelet depletion attenuated the diameter progression of AAA over a 10-day time course by ultrasound tracking (Figure 1 C and D). Further, our data demonstrated enhanced aortic pulse wave velocity (PWV) following initiation of experimental AAA in the control group at day 10 post-surgery suggesting significant structural stiffening effects in the aortic wall. Of note, such changes in aortic PWV were not found in the platelet-depleted group suggesting aggravating effects of platelets with adverse stiffness promoting structural remodeling (Figure 1E). In the thoracic aorta, stable media lamellar units and lack of elastic degradation were found in both groups (Suppl. Figure 1). In addition to the effects seen in the structural architecture of the AAA wall, our findings demonstrated that platelets and macrophages were recruited into the AAA wall at 3 days post-surgery. Platelet depletion reduced the number of macrophages in the AAA wall, suggesting potential modulating effects of platelets in the inflammatory process following murine AAA induction (Figure 1F). In line with this finding, inflammatory gene expression analysis of whole AAA tissue explants revealed downregulation of major inflammatory genes in the platelet depletion group versus the control antibody group at 3 days post-surgery (Figure 1G).

Platelet depletion reverses adverse remodeling of the extracellular matrix. We next analyzed platelet-associated adverse remodeling effects on the extracellular matrix (ECM) of the AAA wall. Our results revealed that the murine AAA wall showed fragmented, and at given locations completely disrupted, elastin membranes within the tunica media by transmission electron microscopy (TEM) (Figure 2 A, B). To examine the impact of platelets on elastin membrane integrity, histological evaluation of AAA explants was performed. Our results show that the intima media thickness of the AAA wall of platelet-depleted mice was thinner when compared to control mice at 10 days post-surgery (Figure 2C). Additionally, the aortic tissue displayed less fragmentation of elastin membranes in AAA explants of platelet-depleted versus control mice (Figure 2D).

These morphologic findings were supported by a partially altered structural gene expression profile in AAA of platelet-depleted mice. In detail, AAA whole tissue explants of platelet-depleted mice revealed reduced expression levels of matrix metalloproteinase (*Mmp*)*9*, *collagen I* and *III* while *Mmp2* and *elastin* (*Eln*) expression was unaltered (Figure 2E). MMP9 is considered a major elastolytic enzyme that reduces resilience and elasticity of conduit arteries and was downregulated in whole AAA explants of platelet depleted vs. control mice at 10 days post-surgery (Figure 2E), consistent with the aforementioned reduced elastin

fragmentation in the same group. Notably, we found that osteopontin (*Spp1*/OPN), a multifunctional and highly phosphorylated glycoprotein was up-regulated at the gene expression level in aortic tissue of PPE-operated mice and in the plasma following murine experimental AAA induction. *Spp1* expression was down-regulated within the AAA wall of platelet-depleted mice compared to control mice, and OPN protein was reduced in the plasma (Figure 2F and G).

Platelets alter gene expression in macrophages. Since OPN was altered at the transcriptional and protein level upon platelet-depletion, we elected to study the major source of OPN. We incubated M1 macrophages (THP-1 cells), aortic vascular smooth muscle cells (hAoVSMC) and aortic fibroblasts (hAoF) with the releasates of ADP or CRP stimulated platelets. Our results demonstrated that macrophages are the major cell type with the highest *SPP1* expression when compared to resident cells of the AAA wall, such as hAoVSMC and hAoF (Figure 3A). Although platelets themselves carry OPN (Figure 3B), macrophages remained the primary source for OPN protein and *SPP1* gene expression *in vitro* (Figure 3C and D). To study whether platelets are capable of altering gene expression in macrophages, we exposed cell cultures of M1 macrophages to releasates of activated platelets *in vitro* (Figure 3E and F). The data revealed that platelet releasates alter inflammatory gene expression in M1 macrophages. Activated platelet releasates caused marked up-regulation of key inflammatory genes, such as Interleukins *(IL)-6*, *-12B* and *-1B* (Figure 3E). We next studied the influence of releasates on stiffness-related gene expression in M1 macrophages. The activated supernatant of platelets enhanced gene expression of *SPP1* and *MMP9* in M1 macrophages (Figure 3F), which supports our *in vivo* findings and suggests that interactions between platelets and macrophages may be a central mechanism for AAA initiation and diameter progression.

Platelet activation and pro-coagulant activity are key elements for the progression of experimental AAA. We next examined if aberrant platelet activation is responsible for platelet-mediated effects on inflammation and remodeling in AAA. To this end, we determined platelet integrin $\alpha_{IIb}\beta_3$ activation and P-selectin exposure as marker for degranulation using flow cytometry. As shown in figure 4A, blood was drawn at various time points (3d, 10d and 28d post-surgery) (Figure 4A) and aneurysm formation was monitored over a time period of 28 days after PPE surgery and compared to sham-operated controls (Figure 4B). At an early time point (day 3), slightly reduced P-selectin exposure and integrin activation but unaltered phosphatidylserine (PS) exposure were observed following platelet stimulation with PAR4 peptide that activated the thrombin receptor PAR4 (Figure 4C). At 10 days post PPE surgery, no differences in the activation or pro-coagulant activity were detected in platelets from PPE mice compared to sham controls (Figure 4D). However, at a later time point (day 28), we detected significantly enhanced P-selectin exposure and integrin $\alpha_{IIb}\beta_3$ activation after

stimulation of the collagen receptor GPVI using CRP. In addition, pro-coagulant activity of platelets isolated from PPE mice was enhanced compared to sham controls (Figure 4E).

Determination of Spearman's correlation between the diameter of the aneurysm and Annexin V binding to platelets at days 3 and 28 after PPE surgery revealed a strong correlation between aortic diameter expansion and elevated pro-coagulant activity (Figure 4F) emphasizing a role for PS at the platelet surface in AAA pathology. Notably, the number and size of platelets (Suppl. Figure 2A-C), and the exposure of integrins at the platelet surface under resting and stimulated conditions (Suppl. Figure 2D–E) were not altered at days 3, 10 and 28 after induction of AAA compared to sham controls. Furthermore, elevated platelet-neutrophil conjugates were detected in PPE mice at day 3 post-surgery compared to sham controls (Figure 4G) while no alterations were determined when we analyzed leukocyte-platelet conjugates (Suppl. Figure 2F).

Discussion

In this study, we found that platelets play a crucial role in AAA likely due to modulation of inflammation and degradation of the ECM. Platelet depletion in experimental AAA reduced inflammation and aortic remodeling, leading to significantly reduced aortic diameter expansion in these mice. In experimental mice, platelet activation and pro-coagulant activity was enhanced and might be responsible for platelet-induced effects on AAA pathology.

AAA is a multifactorial disease, which is characterized by chronic inflammation and degradation of the ECM in the abdominal aortic wall, often accompanied by the formation of an ILT. Increased platelet activation and aggregation is a characteristic of many cardiovascular diseases (CVDs), increasing the risk for thromboembolic events (13, 20-23). Here, we provide evidence for enhanced platelet activation at later time points in mice with experimental AAA (PPE mice). PPE mice exhibit elevated platelet responses after stimulation of the major collagen receptor GPVI using CRP, especially with low concentrations of the agonist. This, together with elevated platelet activation in resting, non-stimulated platelets suggests that the threshold to induce platelet responses is reduced in experimental mice with AAA.

Recently, enhanced platelet reactivity (only P-selectin, no integrin activation) has been detected following thrombin and thromboxane receptor activation using platelets from AAA patients and experimental mice (24). The authors used human platelets from healthy participants at any age as controls (not age-matched) and murine platelets isolated from a mouse model with topical application of elastase to induce AAA. In addition, they analyzed the thrombin/thromboxane receptor pathway in murine and human platelets but did not stimulate platelets with ADP or collagen/CRP to activate the major collagen receptor GPVI. Another study from Robless and colleagues detected elevated spontaneous platelet aggregation in AAA patients and in patients with peripheral artery disease (PAD), suggesting enhanced platelet activation even in the absence of agonists (25). No differences were observed in PAC-1 binding or P-selectin exposure in resting platelets of patients with AAA or PAD. This is striking because the conformational change of integrin $\alpha_{IIb}\beta_3$ in its active form is a prerequisite for (spontaneous) platelet aggregation (26). In another study, high glycocalicin levels were detected in patients with AAA, suggesting increased platelet destruction due to elevated platelet activation in these patients. Consequently, the authors detected decreased platelet counts (27). An increase in platelet activation was also observed after endovascular repair of AAA (28), while our analysis of platelet activation in AAA patients occurred before any treatment.

In addition to enhanced platelet activation in PPE mice, we detected elevated PS exposure at the surface of platelets as a marker for pro-coagulant activity. Enhanced pro-coagulant activity

might result from elevated platelet activation. However, it has been shown that inflammatory cytokines may enhance pro-coagulant activity of platelets (29). Pro-coagulant activity of resting and activated platelets might be responsible for elevated thrombin plasma levels in AAA patients (30, 31) which is a common feature. Thus, it is not surprising that there is a strong correlation between elevated pro-coagulant activity of platelets (PS exposure) and aortic diameter expansion in PPE mice (Figure 4F).

So far, a small number of experimental studies have analyzed the role of platelets in AAA. Touat and colleagues used a xenograft model of rats to induce aneurysms (17). They showed that platelet inhibition by abciximab (which blocks integrin $\alpha_{IIb}\beta_3$) limited aortic aneurysm expansion, suggesting that platelet stimulation, and in particular integrin $\alpha_{IIb}\beta_3$ activation, may be a promising target in the prevention of AAA progression. To date, platelet responses have been analyzed mainly in the Ang-II infusion model. Liu and colleagues showed that treatment of mice with clopidogrel, an inhibitor of the ADP receptor $P2Y_{12}$, prevents Ang-II induced AAA formation by protecting the elastic cell lamina in the mouse aorta. Further, the authors found reduced macrophage infiltration and MMP2 expression after clopidogrel treatment (32). In a more recent study, Owens and colleagues found reduced rupture of established AAAs and improved survival of mice after clopidogrel treatment (15). However, all these studies have been done in Ang-II infused mice, an experimental model that has been shown to primarily feature aortic dissection as a precursor to aortic aneurysm formation. In agreement with these results obtained from Ang-II infused mice, we detected reduced inflammation and reduced elastin fragmentation in platelet-depleted PPE mice, suggesting that platelet-mediated processes play a role in both, aortic dissection and aortic aneurysm formation.

In contrast, a recent study of Liu and colleagues provided evidence for a protective effect of platelets in the Ang-II induced mouse model, in which platelet infusion significantly reduced aortic diameter elevation and inflammatory responses (33). However, differences in experimental design and the fact that the Ang-II infusion model is a dissection model in comparison to the PPE model that mimics human AAA pathology might be responsible for differences in results. Interestingly, one study of P-selectin knock-out mice has utilized the PPE mouse model (34). Genetic deficiency of P-selectin was shown to be protective, as these mice showed attenuated aneurysm formation after infusion with porcine pancreatic elastase. However, the authors claim that P-selectin deficiency resulted in reduced inflammation and aortic wall remodeling according to abdominal aortic tissue samples from day 14 which have been stained with either hematoxylin/eosin, Masson's trichrome or Verhoff’s van Gieson. Moreover, P-selectin is exposed not only at the platelet but also at the endothelial membrane. Thus, the presented effects on inflammation and remodeling cannot be attributed solely to platelets and would need to be verified using techniques other than histology.

In summary, own data as well as results from different groups highly support the potential for antithrombotic/antiplatelet strategies in patients to modulate the progression and rupture of AAA. It will be of great importance to identify druggable targets to limit platelet activation and pro-coagulant activity for this purpose.

Methods

Cell culture of human cell lines. The human aortic fibroblasts (hAoF) and THP-1 were cultured in T-75 flasks in 15 mL of their respective media (fibroblast growth medium, Sigma-Aldrich, #C23010), RPMI 1640 medium (Gibco™, #21875034) including 10% fetal bovine serum (FBS) superior (Sigma-Aldrich, #S0615) and 1% penicillin-streptomycin (Gibco™, #15140122). At 70-80% confluence, cells were split 1:5. For this purpose, adherent hAoF were washed twice with DPBS and dissolved from soil with Trypsin-EDTA (Sigma-Aldrich, #T3924). Trypsinization was stopped with medium, and the cell suspension was transferred to a Falcon and centrifuged at 200 *g* for 5 min. The supernatant was discarded and the cells were resuspended in fresh medium. THP-1 cells do not require trypsinization and were immediately transferred into a falcon. Before resuspension in fresh medium the cells were washed once with DPBS by an additional centrifugation step at 200 *g* for 5 minutes. Taken up in fresh medium, the cells were ready for cell culture experiments.

For cell culture experiments, cells were seeded into a 24-well plate at 1.5 x 10^5 cells/well. HAoF were incubated for 24 h at 37 °C and 5% CO_2 to allow the cells to become adherent. THP-1 cells were differentiated into M1 macrophages by incubation with phorbol-12-myristat-13-acetat (PMA, 8.12 nM) (Sigma-Aldrich, #P1585) for 24-48 h followed by incubation with IFN-γ (20 ng/mL) (R&D systems, #285-IF) and lipopolysaccharide (LPS, 100 ng/ml) (Sigma-Aldrich, #L3012) for 24 h. Once hAoF and M1 macrophages became adherent, the platelet supernatant was added and the samples were incubated at 37 °C and 5% CO_2 for 6 h. Afterwards, the supernatant was discarded and the cells were washed twice with ice-cold DPBS. Finally, the cells were detached from wells using TRI Reagent® (Sigma-Aldrich, #T9424).

Gene expression from human platelets and cell lysates of M1 macrophages. Human platelets were isolated from platelet concentrates following the described protocol. 1-5 x 10^9 platelets were centrifuged at 2500 *g* for 5 min at 4 °C. The supernatant was discarded and the pellet was resuspended in TRI Reagent®. After transferring the sample into a DNA LoBind Tube (Eppendorf, #30108051), Chloroform (Sigma-Aldrich, #372978) was added at a ratio of 1:5. The samples were shaken thoroughly, incubated for 3 min at RT and centrifuged at 12,000 *g* for 15 min at 4 °C. The aqueous phase was diluted in pure ethanol (3-fold) and mixed with linear acrylamide (1:500) (Invitrogen, #AM9520). After an incubation at 4 °C overnight, the samples were centrifuged at 21,130 *g* at 4 °C. The supernatant was discarded, the pellet washed in ice-cold 80% ethanol and resuspended in 25 µL nuclease free water. Total RNA from cell culture lysates of M1 macrophages was isolated using the RNeasy Mini Kit (Qiagen, #74106) according to the manufacturer's protocol. RNA content and quality were measured using the BioPhotometer D30 (Eppendorf). All samples were adapted to the same amount of RNA. DNA digestion was performed with DNAse I (Roche, #04716728001) according to the

following protocol: 30min/37 °C; 10min/75 °C using a PCR thermocycler (Eppendorf). Subsequent cDNA synthesis was performed using the ImProm- II™ Reverse Transcription System (Promega, #A3800) according to their protocol. For quantification of mRNA levels, fast SYBR™ Green Master Mix (Applied Biosystems, #4385612) was used with following specific oligonucleotide primers: MMP2 (PPH00151B-200), MMP9 (PPH00152E-200), COL1A1 (PPH01299F-200), COL3A1 (PPH00439F-200), SPP1 (PPH00582E-200), and GAPDH (PPH00150F-200) acquired from Qiagen. Following oligonucleotide primers were acquired from Origene: MCP1 (HP 206587), IL-6 (HP 200567), IL-12β (HP 205923), TNF-α (HP 200561), IL-10 (HP 200540) and IL-8 (HP 200551). The IL-1β primer pair (frwd: AGCTTCCTTGTGCAAGTGTCTGAG, rev: TGTTGATGTGCTGCTGCGAGAT) were purchased from Eurofins. Data are normalized to GAPDH and fold changes were calculated using the $^{\Delta\Delta}$Ct method.

Experimental AAA models. 10-week-old standard C57BL/6J mice were purchased through Jackson or Janvier Lab. To induce experimental AAA, mice were anesthetized with 2-3% isoflurane and received a locally subcutaneous (s.c.) injection of buprenorphine (0.1 mg/kg) (Temgesic, Eumedica) 30 min before surgery. After median laparotomy, the proximal and distal infrarenal aorta were temporarily ligated to create an aortotomy above the iliac bifurcation. A catheter was inserted into the distal end of the aortotomy and used to infuse the aorta with sterile isotonic saline (NaCl, 0.9%) containing type I Porcine Pancreatic Elastase (2.5 U/mL) (Sigma-Aldrich, #E1250) at 120 mm Hg for 5 min. The vessels in control mice were infused with sodium chloride only. After removal of the infusion catheter, the aortotomy was closed without constriction of the aortal lumen. Finally, the abdomen was closed. For pain relief, all animals received Buprenorphine s.c. every 6 h during the daylight phase for three days and in the dark phase via drinking water (0.3 µg/mL). At the endpoints of the experiments (3, 10, 28 days), mice were euthanized by terminal heart puncture under deep isoflurane anesthesia followed by cervical dislocation.

Mice for the depletion experiments were injected with platelet depletion antibody (Emfret Analytics, polyclonal anti-GPIb alpha #R300) and a corresponding IgG antibody (Emfret Analytics, #C301) as controls after surgery (0d and 5d). Endpoints of the experiments were day 3 and 10 post-(PPE)surgery.

Ultrasound imaging. Prior PPE surgery (baseline) and at days 3, 7, 10, 14, 21 and 28 following surgery, maximal aortic diameters at the aneurysm site were measured using ultrasound. Mice were anaesthetized with 2-3% isoflurane, placed on a 37 °C heated plate and ultrasound imaging was performed using a Vevo 2100® High-Resolution In Vivo Micro-Imaging System (VisualSonics). Inner diameter-measurements were obtained following a standardized imaging algorithm with longitudinal B-Mode images during the systolic phase. PWV was examined to

assess aortic stiffness by simultaneous tracking of the ECG and the pulse wave at the aortic bifurcation (bif). The distance from the aortic valve to the bif was measured during sacrifice and was set to 3.98 cm for further calculations. For each mouse, 5 PW Doppler sets were recorded. In each set, 3 measurements from the foot of the R-wave of the ECG to the offspring of the pulse wave at the bif were measured to determine the transit time between these two locations. Global aortic PVW was estimated as a ratio of the distance (d) and time (t) delay of the pulse wave between both locations.

Platelet preparation and total blood cell count in mice. Murine blood was collected by heart puncture of the right ventricle and transferred into a heparin solution (20 U/mL). Platelet count and mean platelet volume (MPV) were determined using a hematology analyzer (Sysmex KX-21N, Norderstedt, Germany). For platelet preparation, the blood was centrifuged at 250 *g* at RT for 5 min. Then the supernatant was centrifuged again at 50 *g* for 6 min. To extract platelet-rich plasma (PRP), the supernatant of the last step was centrifuged with apyrase (0.02 U/mL) and prostacyclin (PGI_2, 0.5 µM) at 650 *g* at RT for 5 min. Plasma samples were stored at -70°C for later experiments. The platelet pellet was resuspended and washed twice in murine Tyrode's buffer (136 mM NaCl, 0.4 mM Na_2HPO_4, 2.7 mM KCl, 12 mM $NaHCO_3$, 0.1% glucose, 0.35% BSA, pH 7.4) supplemented with PGI_2 (0.5 µM) and apyrase (0.02 U/mL) by centrifugation at 650 *g* at RT for 5 min. Finally, platelets were resuspended in Tyrode's buffer and incubated at 37 °C until use.

EM microscopy. Aortic tissue was harvested from PPE mice. Briefly, aorta was perfused with heparin (180 units/15 mL PBS) from left ventricle (butterfly puncture) to right atrium (incision). Perfuse with 4% PFA (in PBS pH 7.4) with slow steady hand syringes.

Afterwards, aortic tissue was fixed with a solution of 2% glutaraldehyde and 2% paraformaldehyde in cacodylate buffer (0.1 M, pH 7.2) at RT overnight. The next day, samples were washed twice in sodium cacodylate buffer (0.1 M) at RT for 10 min, post-fixed with 2% aqueous osmium tetroxide (OsO_4) at RT for 5 h, washed twice with milliQ water and stained *en bloc* with 4% uranyl acetate overnight. After dehydration through a graded ethanol series and propylene oxide, the tissue was infiltrated and embedded in 100% Eponate 12 resin (Ted Pella, Inc., Redding, CA, USA). Polymerization was performed at 60 °C for 24 h. Ultrathin sections were cut using a Leica Ultracut microtome (Leica, Deerfield, IL) and then post-stained with Reynolds lead citrate. The stained samples were examined in a FEI Tecnai G2 Spirit BioTWIN transmission electron microscope (Hillsboro, OR) operated at 80kV. Electron micrographs were taken with an AMT XR41 CCD camera from Advanced Microscopy Techniques, Corporation (Woburn, MA).

Gene expression of murine aortic tissue. Total RNA was isolated from murine aortae with a TRIzol-based (Invitrogen) RNA isolation protocol. RNA was quantified by NanoDrop (Agilent

Technologies), and RNA and miRNA quality were verified with the Agilent 2100 Bioanalyzer (Agilent Technologies). Samples required 260/280 ratios of >1.8 and sample RNA integrity numbers of ≥9 for inclusion. RNA was reverse-transcribed with the TaqMan MicroRNA Reverse Transcription kit (Applied Biosystems) according to the manufacturer's instructions. To quantitate the mRNA levels the TaqMan qRT-PCR assay was used. Following specific oligonucleotide primers were purchased by Thermo Fisher Scientific:

Il-1β (Mm00434228_m1), *Il-6* (Mm00446190_m1), *Il-8* (Mm00441263_m1), *Il-10* (Mm01288386_m1), *Il-12β* (Mm01288989_m1), *Ccl2* (Mm00441242_m1), *Tnf-α* (Mm00443258_m1), *Eln* (Hs00355783_m1), *Mmp2* (Mm00439498_m1), *Mmp9* (Mm00442991_m1), *Col1a1* (Mm00801666_g1), *Col3a1* (Mm01254476_m1), *Spp1* (Mm00436767_m1), *18S* (4319413E). Data are normalized to 18S or GAPDH and all fold changes were calculated using the $^{\Delta\Delta}$Ct method.

Flow cytometry. For flow cytometry heparinized mouse blood was washed twice at 250 *g* for 5 min by discarding the supernatant and resuspending the blood pellet in murine Tyrode's buffer (136 mM NaCl, 0.4 mM Na_2HPO_4, 2.7 mM KCl, 12 mM $NaHCO_3$, 0.1% glucose, 0.35 % BSA, pH 7.4). Finally, the pellet is diluted in mouse Tyrode's buffer including $CaCl_2$ (2 mM). Blood samples were mixed with antibodies and stimulated with indicated agonists at RT for 15 min in the dark. Reaction was stopped by the addition of DPBS and samples were analysed on a FACSCalibur flow cytometer (BD Biosciences).

Briefly, two-colour analysis of murine platelet activation was performed using fluorophore-labeled antibodies for P-selectin expression (Emfret Analytics, Wug.E9-FITC, #M130-1) and the active form of $\alpha_{IIb}\beta_3$ integrin (Emfret Analytics, JON/A-PE, #M023-2). For analysis of α_5 glycoprotein surface expression and up-regulation as well as activation of integrin β_3 expression blood samples were mixed with specific antibodies (Emfret Analytics, β_3 chain, GPIIIa, Luc.H11-FITC, #M031-1 or Integrin α_5/CD49e, Tap.A12-FITC, BD Biosciences) and incubated for 15 min at RT in the dark. For the analysis of CD45- and Ly6G-platelet aggregates specific antibodies were used (Emfret Analytics, GPIb/CD42b, Xia.G5-PE; BD Biosciences, anti-mouse CD45-APC, #559864 and BioLegend, anti-mouse Ly-6G-APC, #127614).

For detection of phosphatidylserine (PS) exposure Cy™5 AnnexinV (BD Biosciences) were used – staining was performed while binding buffer (10 mM Hepes, 140 mM NaCl, 2.5 mM $CaCl_2$, pH 7.4) was used instead of DPBS.

Histology. For the analysis of platelets in aortic tissue of PPE mice, 5-7-micron sections of paraffin-embedded tissue were prepared.

Hematoxylin and eosin staining of murine aortic tissue. Hematoxylin and eosin staining was performed using a common HE-staining protocol (42).

Immunofluorescence staining. For immunofluorescence staining of platelets (CD42b) and macrophages (Mac-3), sections of murine aortic walls were stained. For staining of murine aortic wall paraffin-embedded tissue was used. Prior to the staining the paraffin-embedded sections were deparaffinized and hydrated. For antigen unmasking tissue was microwaved at 360 kW for 10 min. For the blocking of nonspecific binding sites, paraffin-embedded sections were incubated with DPBS + 0.3 % Triton x-100 and goat serum (5%) at RT for 1 h. The primary antibodies, CD42b monoclonal antibody (20 µg/mL, Invitrogen™, #42C01), BD Pharmingen™ purified mouse IgG1 κ isotype control (50 µg/mL, BD Bioscience, #554121), BD Pharmingen™ purified rat anti-mouse Mac-3, unlabeled (3.125 µg/mL, BD Bioscience, #BDB550292), purified rat anti-mouse GPIbα (CD42b, 10 µg/mL, Emfret Analytics, #M042-0)) were incubated at 4 °C overnight. On the next day, the appropriate secondary antibodies (goat anti-rabbit IgG (H+L) cross-adsorbed secondary antibody, Alexa Fluor™ 555 (20 µg/mL, Invitrogen™, #A-21428), eBioscience™ streptavidin eFluor™ 660 conjugate (10 µg/mL, Invitrogen™, #50-4317-80)) were applied to the tissue at RT for 1 h. In case of platelet staining with CD42b, an intermediate step of biotinylation was used to enhance the fluorescence signal (goat anti-mouse IgG antibody (H+L), biotinylated, GT (7.5 µg/mL, Vector Laboratories, #VEC-BA-9200), goat anti-rat IgG antibody (H+L), biotinylated (7.5 µg/mL, Vector Laboratories, #BA-9400)). Nuclei were identified using DNA staining with 4, 6 diamidino-2-phenylindole dihydrochloride (DAPI, Roche, 1:3000). Samples were analysed using confocal microscopy (LSM 710, Carl Zeiss, Germany).

Verhoeff van Gieson staining. Using a modified Elastin Verhoeff van Gieson staining (VVG) according to manufacturer's protocol (abcam, elastic stain kit #ab150667) elastin layers were visualized. Elastin fragmentation was determined as elastin fragments / media lamellar units via ZEN 3.3. (blue edition) software. The number of these breakdowns were counted in both thoracic and abdominal aortic segments of naive mice, platelet-depleted PPE mice and IgG treated PPE mice (controls).

Quantification of plasma levels of OPN, MMP2 and MMP9. Circulating OPN in plasma of mice was determined according the manufacturer's protocol for Mouse/Rat osteopontin (OPN) Quantikine ELISA Kit (R&D Systems, #MOST00). In addition, OPN content was analyzed in macrophages from cell cultures using the osteopontin/SPP1 ELISA kit (Thermo Fisher Scientific, #EHSPP1) according to the appropriate protocol.

Statistics. Data are provided as arithmetic means ± SEM, statistical analysis was made by GraphPad Prism Version 8.0. Clinical data were initially evaluated to check the normality of the distribution using the Shapiro-Wilk test and subsequently the unpaired t-test with Welch's correction was used. Comparison of two groups were performed using unpaired student's t-test or multiple t-test. Comparisons of more than two groups were performed using a one- or two-

way ANOVA with Sidak's, Holm-Sidak's or Tukey's multiple-comparison correction. *P* values of less than 0.05 were considered significant.

Author contributions

MUW, HS and ME designed the study. MUW, JM, KJK, TF, AE, YHR, MC, NP, CB, WI, IK, and JMS performed experiments. MUW, KJK, MC, and ME analyzed and interpreted data. MUW, KJK and ME wrote the manuscript with all authors providing feedback. MUW, JM and KJK contributed equally to this study.

Acknowledgments

We thank Martina Spelleken for excellent technical assistance, Sandra Szczutkowski and Christos Dimopoulos for histology and platelet adhesion experiments, and the center for Advanced Imaging (CAi) for technical support. The study was funded by the Deutsche Forschungsgemeinschaft (DFG, German Research Foundation), Collaborative Research Centre TRR259 (Aortic Disease)—Grant No. 397484323, TP A07 to HS and ME and Grant No. GZ: WA 3533/3-1 to MUW and EL 651/6-1 to ME.

References

1. Eckstein HH, Böckler D, Flessenkämper I, Schmitz-Rixen T, Debus S, and Lang W. Ultrasonographic screening for the detection of abdominal aortic aneurysms. *Deutsches Arzteblatt international.* 2009;106(41):657-63.
2. Cameron SJ, Russell HM, and Owens AP, 3rd. Antithrombotic therapy in abdominal aortic aneurysm: beneficial or detrimental? *Blood.* 2018;132(25):2619-28.
3. Golledge J, Morris DR, Pinchbeck J, Rowbotham S, Jenkins J, Bourke M, et al. Editor's Choice - Metformin Prescription is Associated with a Reduction in the Combined Incidence of Surgical Repair and Rupture Related Mortality in Patients with Abdominal Aortic Aneurysm. *European journal of vascular and endovascular surgery : the official journal of the European Society for Vascular Surgery.* 2019;57(1):94-101.
4. Karrowni W, Dughman S, Hajj GP, and Miller FJ, Jr. Statin therapy reduces growth of abdominal aortic aneurysms. *Journal of investigative medicine : the official publication of the American Federation for Clinical Research.* 2011;59(8):1239-43.
5. Kunath A, Unosson J, Friederich-Persson M, Bjarnegård N, Becirovic-Agic M, Björck M, et al. Inhibition of angiotensin-induced aortic aneurysm by metformin in apolipoprotein E-deficient mice. *JVS-vascular science.* 2021;2:33-42.
6. Sutton SS, Magagnoli J, Cummings TH, and Hardin JW. Association between metformin and abdominal aortic aneurysm in diabetic and non-diabetic US veterans. *Journal of investigative medicine : the official publication of the American Federation for Clinical Research.* 2020;68(5):1015-8.
7. Sakalihasan N, Limet R, and Defawe OD. Abdominal aortic aneurysm. *Lancet (London, England).* 2005;365(9470):1577-89.

8. Shimizu K, Mitchell RN, and Libby P. Inflammation and cellular immune responses in abdominal aortic aneurysms. *Arteriosclerosis, thrombosis, and vascular biology.* 2006;26(5):987-94.
9. Kazi M, Thyberg J, Religa P, Roy J, Eriksson P, Hedin U, et al. Influence of intraluminal thrombus on structural and cellular composition of abdominal aortic aneurysm wall. *Journal of vascular surgery.* 2003;38(6):1283-92.
10. Wang DH, Makaroun MS, Webster MW, and Vorp DA. Effect of intraluminal thrombus on wall stress in patient-specific models of abdominal aortic aneurysm. *Journal of vascular surgery.* 2002;36(3):598-604.
11. O'Leary SA, Kavanagh EG, Grace PA, McGloughlin TM, and Doyle BJ. The biaxial mechanical behaviour of abdominal aortic aneurysm intraluminal thrombus: classification of morphology and the determination of layer and region specific properties. *Journal of biomechanics.* 2014;47(6):1430-7.
12. Vorp DA, Mandarino WA, Webster MW, and Gorcsan J, 3rd. Potential influence of intraluminal thrombus on abdominal aortic aneurysm as assessed by a new non-invasive method. *Cardiovascular surgery (London, England).* 1996;4(6):732-9.
13. Papapanagiotou A, Daskalakis G, Siasos G, Gargalionis A, and Papavassiliou AG. The Role of Platelets in Cardiovascular Disease: Molecular Mechanisms. *Current pharmaceutical design.* 2016;22(29):4493-505.
14. Busch A, Bleichert S, Ibrahim N, Wortmann M, Eckstein HH, Brostjan C, et al. Translating mouse models of abdominal aortic aneurysm to the translational needs of vascular surgery. *JVS-vascular science.* 2021;2:219-34.
15. Owens AP, 3rd, Edwards TL, Antoniak S, Geddings JE, Jahangir E, Wei WQ, et al. Platelet Inhibitors Reduce Rupture in a Mouse Model of Established Abdominal Aortic Aneurysm. *Arteriosclerosis, thrombosis, and vascular biology.* 2015;35(9):2032-41.
16. Dai J, Louedec L, Philippe M, Michel JB, and Houard X. Effect of blocking platelet activation with AZD6140 on development of abdominal aortic aneurysm in a rat aneurysmal model. *Journal of vascular surgery.* 2009;49(3):719-27.
17. Touat Z, Ollivier V, Dai J, Huisse MG, Bezeaud A, Sebbag U, et al. Renewal of mural thrombus releases plasma markers and is involved in aortic abdominal aneurysm evolution. *The American journal of pathology.* 2006;168(3):1022-30.
18. Lindholt JS, Björck M, and Michel JB. Anti-platelet treatment of middle-sized abdominal aortic aneurysms. *Current vascular pharmacology.* 2013;11(3):305-13.
19. Touat Z, Lepage L, Ollivier V, Nataf P, Hvass U, Labreuche J, et al. Dilation-dependent activation of platelets and prothrombin in human thoracic ascending aortic aneurysm. *Arteriosclerosis, thrombosis, and vascular biology.* 2008;28(5):940-6.
20. Furman MI, Benoit SE, Barnard MR, Valeri CR, Borbone ML, Becker RC, et al. Increased platelet reactivity and circulating monocyte-platelet aggregates in patients with stable coronary artery disease. *Journal of the American College of Cardiology.* 1998;31(2):352-8.
21. Trip MD, Cats VM, van Capelle FJ, and Vreeken J. Platelet hyperreactivity and prognosis in survivors of myocardial infarction. *The New England journal of medicine.* 1990;322(22):1549-54.

22. Zeller JA, Tschoepe D, and Kessler C. Circulating platelets show increased activation in patients with acute cerebral ischemia. *Thrombosis and haemostasis.* 1999;81(3):373-7.
23. Reusswig F, Polzin A, Klier M, Dille MA, Ayhan A, Benkhoff M, et al. Only Acute but Not Chronic Thrombocytopenia Protects Mice against Left Ventricular Dysfunction after Acute Myocardial Infarction. *Cells.* 2022;11(21).
24. Morrell CN, Mix D, Aggarwal A, Bhandari R, Godwin M, Owens P, 3rd, et al. Platelet olfactory receptor activation limits platelet reactivity and growth of aortic aneurysms. *The Journal of clinical investigation.* 2022;132(9).
25. Robless PA, Okonko D, Lintott P, Mansfield AO, Mikhailidis DP, and Stansby GP. Increased platelet aggregation and activation in peripheral arterial disease. *European journal of vascular and endovascular surgery : the official journal of the European Society for Vascular Surgery.* 2003;25(1):16-22.
26. Faull RJ, and Ginsberg MH. Dynamic regulation of integrins. *Stem cells (Dayton, Ohio).* 1995;13(1):38-46.
27. Milne AA, Adam DJ, Murphy WG, and Ruckley CV. Effects of asymptomatic abdominal aortic aneurysm on the soluble coagulation system, platelet count and platelet activation. *European journal of vascular and endovascular surgery : the official journal of the European Society for Vascular Surgery.* 1999;17(5):434-7.
28. Arnaoutoglou E, Kouvelos G, Papa N, Karamoutsios A, Bouris V, Vartholomatos G, et al. Platelet activation after endovascular repair of abdominal aortic aneurysm. *Vascular.* 2016;24(3):287-94.
29. Li J, Tong D, Chen F, Song B, Wang Y, Liu Y, et al. Inflammatory cytokines enhance procoagulant activity of platelets and endothelial cells through phosphatidylserine exposure in patients with essential hypertension. *Journal of thrombosis and thrombolysis.* 2021;51(4):933-40.
30. Sundermann AC, Saum K, Conrad KA, Russell HM, Edwards TL, Mani K, et al. Prognostic value of D-dimer and markers of coagulation for stratification of abdominal aortic aneurysm growth. *Blood advances.* 2018;2(22):3088-96.
31. Wallinder J, Bergqvist D, and Henriksson AE. Haemostatic markers in patients with abdominal aortic aneurysm and the impact of aneurysm size. *Thrombosis research.* 2009;124(4):423-6.
32. Liu O, Jia L, Liu X, Wang Y, Wang X, Qin Y, et al. Clopidogrel, a platelet P2Y12 receptor inhibitor, reduces vascular inflammation and angiotensin II induced-abdominal aortic aneurysm progression. *PloS one.* 2012;7(12):e51707.
33. Liu X, Chen X, Xu C, Lou J, Weng Y, and Tang L. Platelet protects angiotensin II-driven abdominal aortic aneurysm formation through inhibition of inflammation. *Experimental gerontology.* 2022;159:111703.
34. Hannawa KK, Cho BS, Sinha I, Roelofs KJ, Myers DD, Wakefield TJ, et al. Attenuation of experimental aortic aneurysm formation in P-selectin knockout mice. *Annals of the New York Academy of Sciences.* 2006;1085:353-9.
35. Lok ZSY, and Lyle AN. Osteopontin in Vascular Disease. *Arteriosclerosis, thrombosis, and vascular biology.* 2019;39(4):613-22.

36. Lund SA, Giachelli CM, and Scatena M. The role of osteopontin in inflammatory processes. *Journal of cell communication and signaling.* 2009;3(3-4):311-22.
37. Isoda K, Nishikawa K, Kamezawa Y, Yoshida M, Kusuhara M, Moroi M, et al. Osteopontin plays an important role in the development of medial thickening and neointimal formation. *Circulation research.* 2002;91(1):77-82.
38. Mi T, Nie B, Zhang C, and Zhou H. The elevated expression of osteopontin and NF-κB in human aortic aneurysms and its implication. *Journal of Huazhong University of Science and Technology Medical sciences = Hua zhong ke ji da xue xue bao Yi xue Ying De wen ban = Huazhong keji daxue xuebao Yixue Yingdewen ban.* 2011;31(5):602.
39. Bruemmer D, Collins AR, Noh G, Wang W, Territo M, Arias-Magallona S, et al. Angiotensin II-accelerated atherosclerosis and aneurysm formation is attenuated in osteopontin-deficient mice. *The Journal of clinical investigation.* 2003;112(9):1318-31.
40. Schultz G, Tedesco MM, Sho E, Nishimura T, Sharif S, Du X, et al. Enhanced abdominal aortic aneurysm formation in thrombin-activatable procarboxypeptidase B-deficient mice. *Arteriosclerosis, thrombosis, and vascular biology.* 2010;30(7):1363-70.
41. Seizer P, and May AE. Platelets and matrix metalloproteinases. *Thrombosis and haemostasis.* 2013;110(5):903-9.
42. Jarre A, Gowert NS, Donner L, Münzer P, Klier M, Borst O, et al. Pre-activated blood platelets and a pro-thrombotic phenotype in APP23 mice modeling Alzheimer's disease. *Cellular signalling.* 2014;26(9):2040-50.

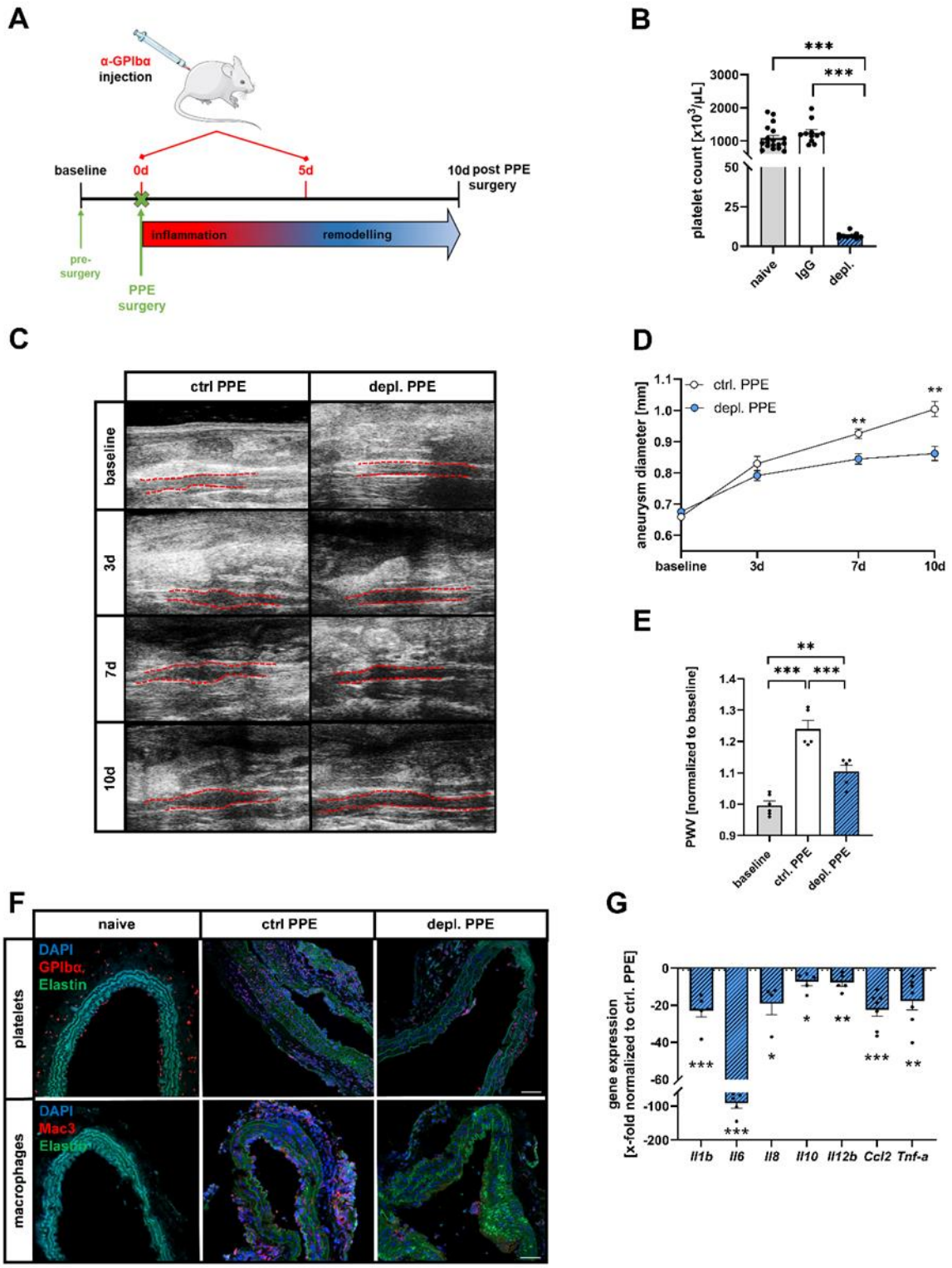

Figure 1. Platelet depletion reduces AAA progression and attenuates inflammatory response. (**A**) Schematic of experimental procedure: C57BL/6J mice received a depleting anti-GPIbα (depl.) or IgG control (ctrl) antibody (at days 0 and 5) after PPE surgery. (**B**) Platelet counts of unoperated mice before and after platelet depletion (n = 11–18). (**C**) Ultrasound images at indicated time points (baseline, days 3, 7 and 10) of platelet-depleted and control mice after PPE surgery to investigate aneurysm development. (**D**) Aneurysm diameter was determined by ultrasound measurements at the indicated time points (n = 4). (**E**) Calculated

pulse wave velocity (PWV) 10 days after PPE surgery, normalized to baseline (n = 5–6). (**F**) Representative immunofluorescence (IF) images of platelets (CD42b/anti-GPIbα, red, upper panels), macrophages (anti-Mac3, red, lower panels), nuclei (DAPI, blue) and elastin (autofluorescence, green) in aortic tissue sections of PPE-operated mice (ctrl PPE or depl. PPE) at day 3 after surgery (n = 4). Aortic tissue of naive mice served as control (n = 4). (**G**) Inflammatory gene expression in aortic tissue of platelet-depleted mice 3 days after PPE surgery. X-fold changes were normalized to control PPE mice (n = 4–7). Data are represented as mean ± SEM. Statistical significances were determined by one-way ANOVA with Holm-Sidak's multiple comparison (**B** and **E**), two-way ANOVA with Sidak's multiple comparison test (**D**) or multiple t-test (**G**). *$P < 0.05$, **$P < 0.01$, ***$P < 0.001$. Scale bar: 50 µm. Ctrl, control; depl., depletion; PPE, porcine pancreatic elastase (infusion); PWV, pulse wave velocity; DAPI, 4′,6-diamidino-2-phenylindole; Il, interleukin; Ccl, CC chemokine ligand; Tnf, tumour necrosis factor.

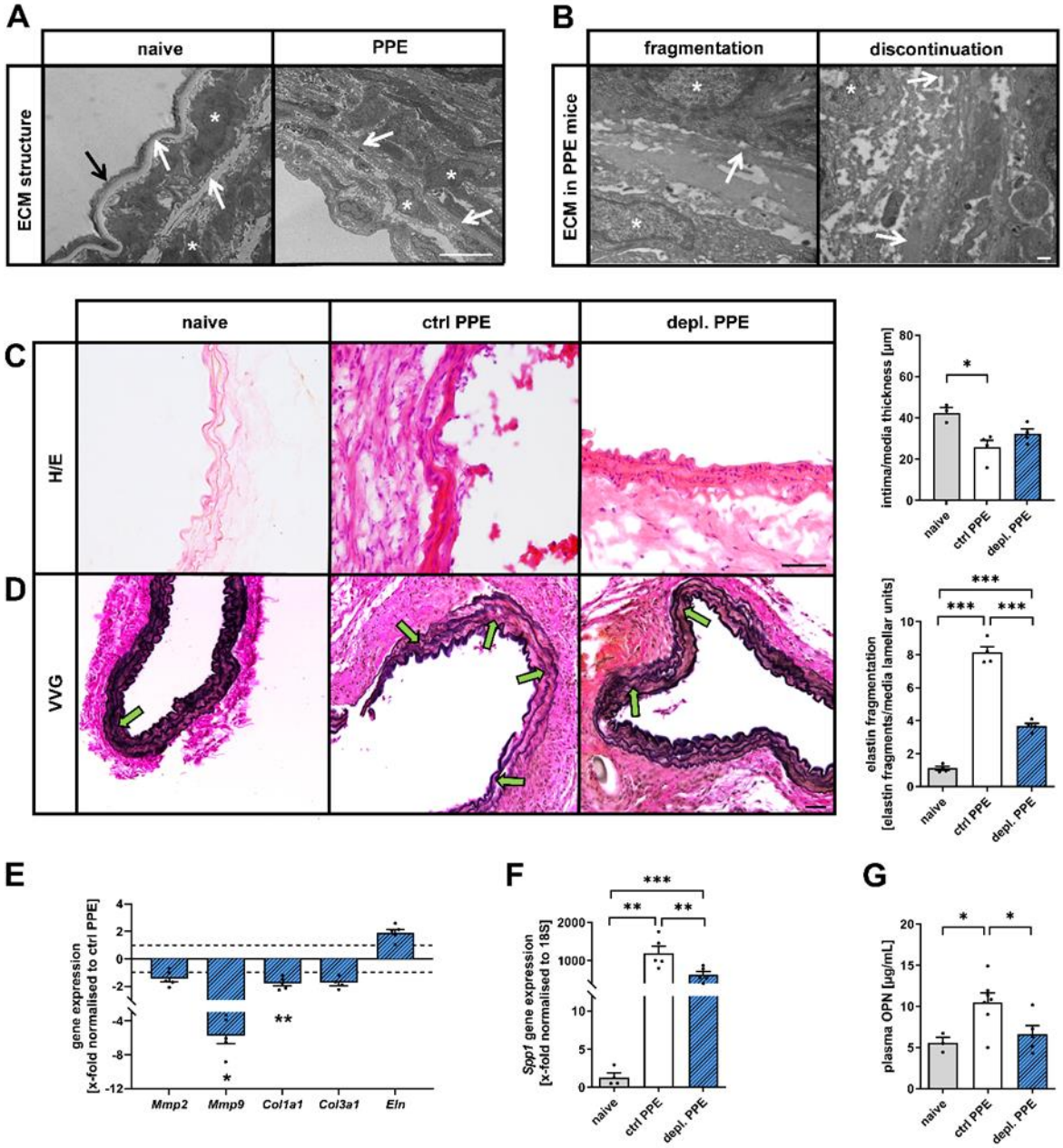

Figure 2. Platelet depletion alters ECM remodeling in PPE-operated mice 10 days after surgery. (**A**) Transmission electron microscopy (TEM) images of aortic tissue from naive and from PPE-operated mice 28 days after surgery (2,900x magnification, n = 2). Black arrow indicate elastin, white arrowheads indicate endothelial layer, and stars indicate vascular smooth muscle cells. (**B**) TEM images of fragmented and discontinuous aortic elastic tissue from mice after PPE surgery (13,000x magnification, n = 2). (**C**–**G**) C57BL/6J mice received a depleting anti-GPIbα (depl.) or IgG control (ctrl) antibody (at days 0 and 5) after PPE surgery and were sacrificed at day 10 for tissue preparation. (**C** and **D**) Representative images of aortic walls from naive and PPE-operated mice using hematoxylin-eosin (H/E) staining (**C**) and Verhoeff van Gieson (VVG) staining (**D**). Intima/media thicknesses were determined after H/E staining (n = 3–4) and elastin fragments (breakdowns) were counted after VVG staining (n =

4). (**E**) Stiffness-related gene expression of aortic tissue in naive and PPE-operated mice. Fold change was normalized to control PPE mice (n = 4–5). (**G**) *Spp1* (OPN) gene expression in aortic tissue of naive and PPE-operated mice. Fold change was normalized to 18S housekeeping gene (n = 4–5). (**H**) Osteopontin plasma concentration (µg/mL) in naive and PPE-operated mice (n = 3–7). Data are represented as mean ± SEM. Statistical significances were determined by one-way ANOVA with Holm-Sidak's multiple comparison test (**C**, **D**, **F** and **G**) and multiple t-test (**E**). *$P < 0.05$, **$P < 0.01$, ***$P < 0.001$. Scale bars: 10 µm (**A**), 0,5 µM (**B**), 50 µm (**C**) and 100 µm (**D**). ECM, extracellular matrix; PPE, porcine pancreatic elastase (infusion); H/E, hematoxylin-eosin; VVG, Verhoeff van Gieson; ctrl, control; depl., depletion; Mmp, matrix metalloproteinase; Col, collagen; Eln, elastin; OPN, osteopontin; *Spp1*, secreted phosphoprotein 1.

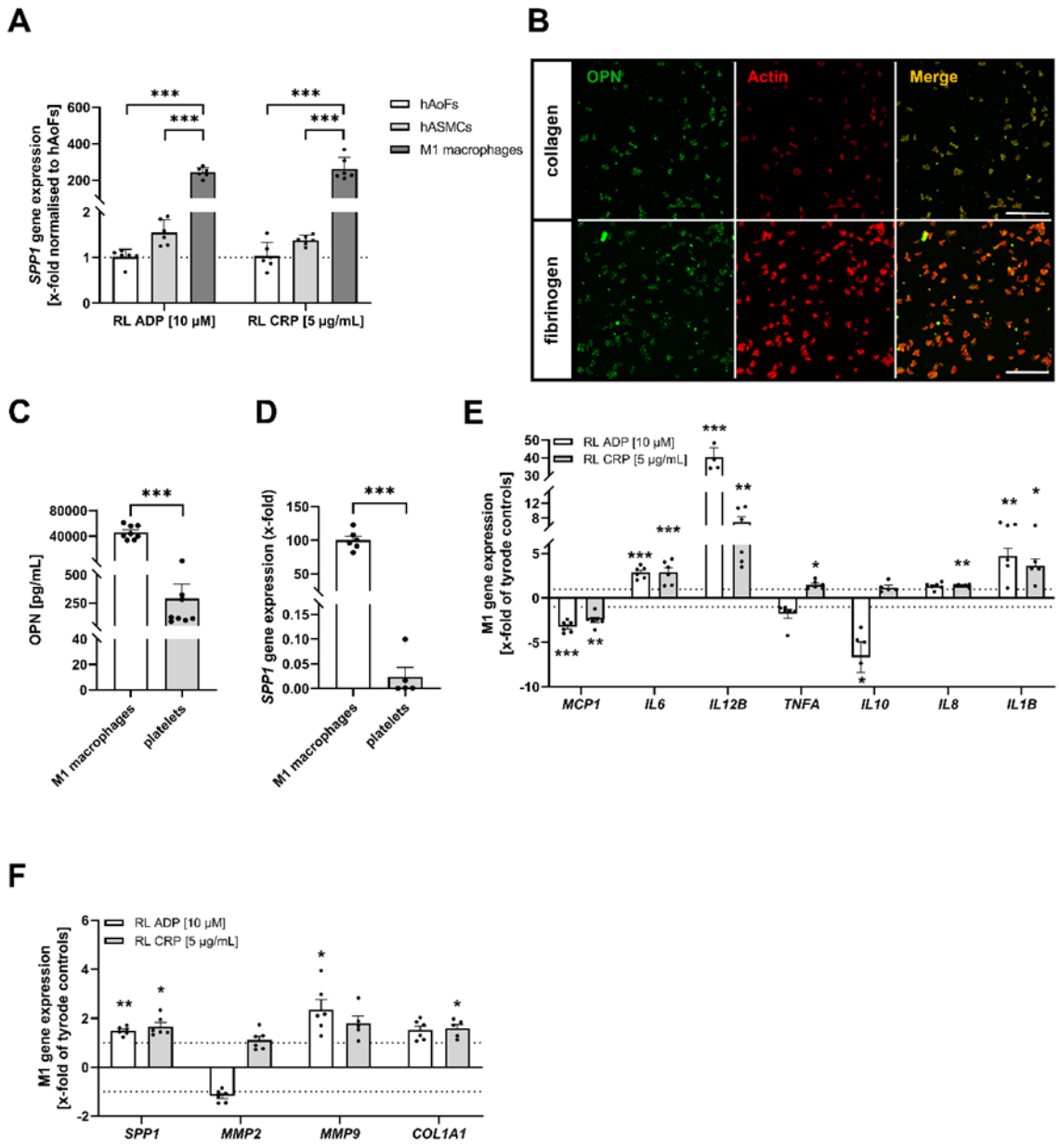

Figure 3. Platelet releasates affect inflammatory and stiffness-related gene expression of M1 macrophages *in vitro.* (**A**) *SPP1* gene expression of hAoFs, hASMCs and differentiated THP-1 cells (M1 macrophages) in cell culture experiments stimulated with releasates (RL) of human platelets after 6 h with indicated agonists (n = 6). Fold changes of hASMCs and THP-1 cells were normalized to hAoFs. (**B**) Representative fluorescence images of OPN (anti-OPN, green) in adherent platelets (actin staining with rhodamine-phalloidin, red) on collagen (200 µg/mL) and fibrinogen (100 µg/mL) after 20 min (n = 3). (**C**) OPN release of differentiated THP-1 cells (M1 macrophages) and platelets after activation with ADP (10 µM) was determined by ELISA (n = 8). (**D**) *SPP1* gene expression in platelets and differentiated THP-1 cells (M1 macrophages) (n = 5–6). (**E** and **F**) Inflammatory and stiffness-related gene expression of differentiated THP-1 cells (M1 macrophages), stimulated with releasates of

human platelets after 6 h with indicated agonist. Fold change was normalized to corresponding Tyrode's control (n = 4–6). Data are represented as mean ± SEM. Statistical significances were determined by two-way ANOVA with Sidak's multiple comparison (**A**), unpaired student's t-test (**C** and **D**) or multiple t-test (**E** and **F**). *$P < 0.05$, **$P < 0.01$, ***$P < 0.001$. Scale bar: 50 µm. *SPP1*, secreted phosphoprotein 1; hAoFs, human aortic fibroblasts; hASMCs, human aortic smooth muscle cells; ADP, adenosine diphosphate; CRP, collagen-related peptide; RL, releasate; OPN, osteopontin; Il, interleukin; MCP, monocyte chemoattractant protein; TNF, tumour necrosis factor; MMP, matrix metalloproteinase; Col, collagen.

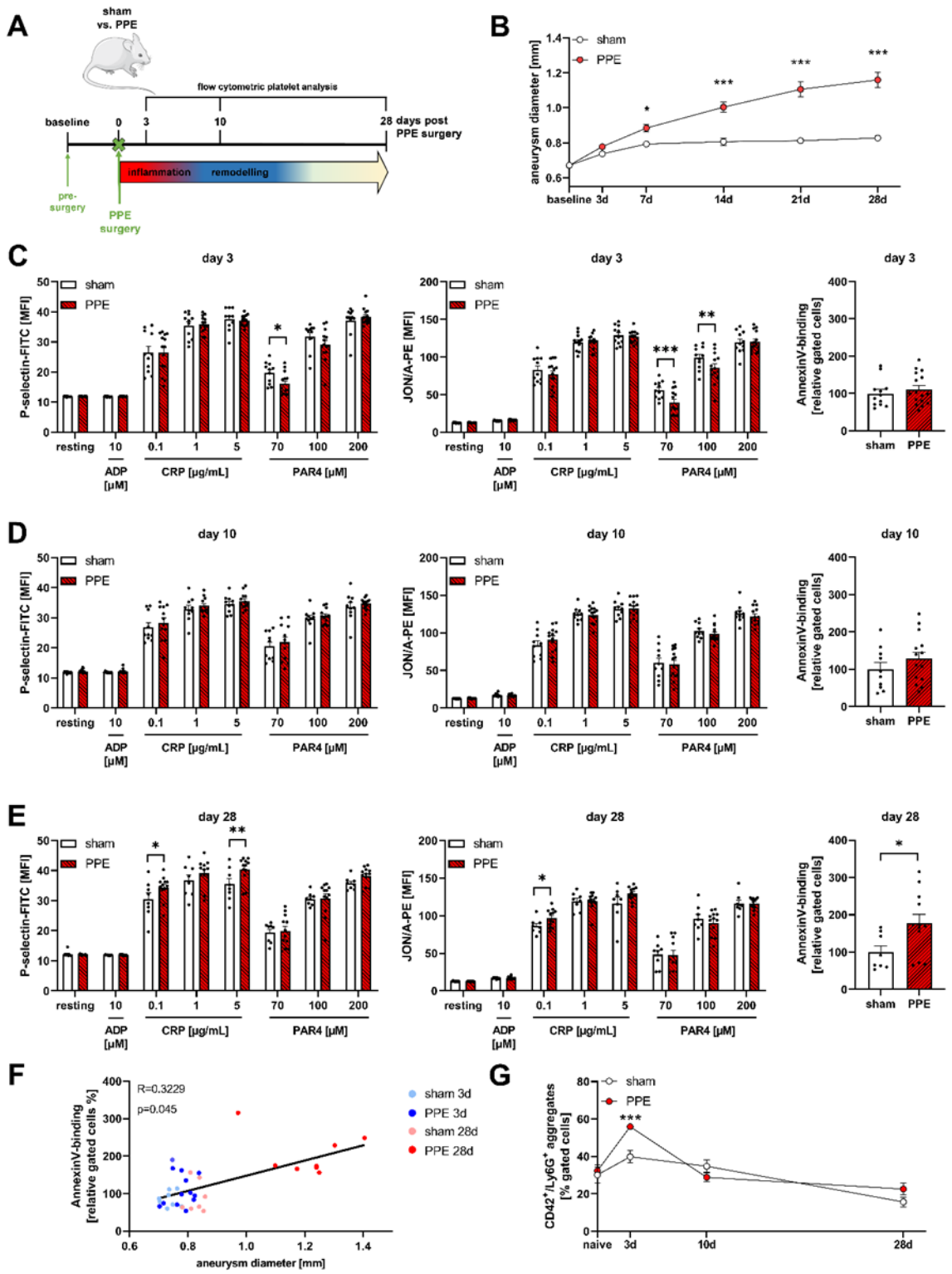

Figure 4. Platelet activation and procoagulant activity is crucial for the AAA progression in the murine PPE model. (**A**) Schematic of experimental procedure: C57BL/6J mice underwent sham or PPE surgery. Mice were sacrificed at indicated time points for flow cytometric analysis of platelets in whole blood at days 3, 10 and 28. (**B**) Ultrasound measurements were performed prior surgery (baseline) and at days 3, 7, 14, 21 and 28 to

investigate aneurysm diameter (n = 8–13). (**C**–**E**) Degranulation marker (P-selectin-FITC), active integrin $\alpha_{IIb}\beta_3$ externalisation (JON/A-PE) and Annexin V binding to platelets from sham- or PPE-operated mice at days 3 (**C**), 10 (**D**) and 28 (**E**) were determined by flow cytometry after stimulation with indicated agonists (n = 7–15). Data are represented as mean or percent-gated cells normalized to control ± SEM. (**F**) Spearman's correlation between the diameter of the aneurysm and Annexin V binding at days 3 and 28 after PPE surgery (n = 8–15). (**G**) Aggregate formation of platelets ($CD42^+$) and neutrophils ($Ly6G^+$) in whole blood of naive, sham- or PPE-operated mice at days 3, 10 and 28 after surgery determined by flow cytometry (n = 5–6). Data are represented as percent-gated cells ± SEM. Statistical significances were determined by two-way ANOVA with Sidak's multiple comparison test (**B** and **G**), unpaired student's t-test or multiple t-test (**C**, **D** and **E**). *$P < 0.05$, **$P < 0.01$, ***$P < 0.001$. PPE, porcine pancreatic elastase (infusion); MFI, mean fluorescence intensity; ADP, adenosine diphosphate; CRP, collagen-related peptide; PAR4, protease-activated receptor 4 activating peptide.